Earth and Planetary Science Letters 449 (2016) 295–301

Contents lists available at ScienceDirect

Earth and Planetary Science Letters

www.elsevier.com/locate/epsl

Macroscopic strength of oceanic lithosphere revealed by ubiquitous fracture-zone instabilities

Cécilia Cadio [a,b,*], Jun Korenaga [a]

[a] Department of Geology and Geophysics, Yale University, 210 Whitney Ave, New Haven, CT 06511, USA
[b] Géosciences Montpellier, Université Montpellier II and CNRS UMR 5243, cc060 Place E. Bataillon, 34095 Montpellier Cedex 05, France

A R T I C L E   I N F O

Article history:
Received 3 October 2015
Received in revised form 9 May 2016
Accepted 20 May 2016
Available online xxxx
Editor: P. Shearer

Keywords:
plate tectonics
upper mantle rheology
convective instabilities
geoid anomalies

A B S T R A C T

The origin of plate tectonics is one of the most fundamental issues in earth and planetary sciences. Laboratory experiments indicate that the viscosity of silicate rocks is so strongly temperature-dependent that the entire surface of the Earth should be one immobile rigid plate. The rheology of oceanic lithosphere is, however, still poorly understood, and there exist few constraints on the temperature dependency of viscosity on the field scale. Here we report a new kind of observational constraint based on the geoid along oceanic fracture zones. We identify a large number of conspicuous small-scale geoid anomalies, which cannot be explained by the standard evolution model of oceanic lithosphere, and estimate their source density perturbations using a new Bayesian inversion method. Our results suggest that they are caused most likely by small-scale convection involving temperature perturbations of $\sim$300 K $\pm$ 100 K. Such thermal contrast requires the activation energy of mantle viscosity to be as low as 100 ± 50 kJ mol^{-1} in case of diffusion creep, and 225 ± 112 kJ mol^{-1} in case of dislocation creep, substantially reducing the thickness of the stiffest part of oceanic lithosphere. Oceanic lithosphere may thus be broken and bent much more easily than previously thought, facilitating the operation of plate tectonics.

© 2016 Elsevier B.V. All rights reserved.

1. Introduction

The rheology of oceanic lithosphere plays a major role in the operation of plate tectonics, a phenomenon only observed on our planet and still considered enigmatic (Bercovici et al., 2000; Tackley, 2000; Schubert et al., 2001). Oceanic lithosphere, which is the top boundary layer of mantle convection, is generally thought to be very stiff, and thus difficult to break or bend. The Earth's mantle is composed of silicate rocks, whose viscosity is strongly temperature-dependent (Karato and Wu, 1993; Hirth and Kohlstedt, 2003). This dependency is quantified by the activation energy, which is usually estimated to range from 240–375 kJ mol^{-1} (diffusion creep) to 470–510 kJ mol^{-1} (dislocation creep) for the upper mantle in wet and dry conditions respectively, based on the deformation experiments of olivine aggregates (Mei and Kohlstedt, 2000a, 2000b; Karato and Jung, 2003; Hirth and Kohlstedt, 2003). With this value, the bulk of the oceanic lithosphere is too stiff to become convectively unstable, prohibiting the initiation of subduction (Solomatov, 1995). In order to generate plate tectonics, therefore, some additional mechanism is required to compensate temperature-dependent viscosity, but what this mechanism could be is still unresolved (Bercovici, 2003; Korenaga, 2013). So far proposed mechanisms include the feedback between shear localization and grain size evolution (Kameyama et al., 1997; Braun et al., 1999; Landuyt et al., 2008), the pre-existing zone of weakness such an oceanic fracture zone (Toth and Gurnis, 1998; Hall et al., 2003; Gurnis et al., 2004), the higher water content of oceanic lithosphere (e.g. Regenauer-Lieb et al., 2001), hydration by thermal cracking (Korenaga, 2007), and rheological weakening by a secondary orthopyroxene phase (Farla et al., 2013).

Observational constraints on the temperature dependency of viscosity have been difficult to establish. The geodynamic study of seamount loading history suggests the activation energy of 120 kJ mol^{-1} for diffusion creep (Watts and Zhong, 2000), but this is usually thought to represent the temperature dependency of the Peierls mechanism (Goetze and Evans, 1979), not that of high-temperature creep. The Peierls mechanism can operate only under low temperatures and very high stresses (>100 MPa), so it is not relevant to the destabilization of oceanic lithosphere by low convective stresses, which is often believed to be critical for

* Corresponding author at: Géosciences Montpellier, Université Montpellier II and CNRS UMR 5243, cc060 Place E. Bataillon, 34095 Montpellier Cedex 05, France. Tel.: +33 4 67 14 34 87.
E-mail addresses: Cecilia.Cadio@gm.univ-montp2.fr (C. Cadio), jun.korenaga@yale.edu (J. Korenaga).

http://dx.doi.org/10.1016/j.epsl.2016.05.027
0012-821X/© 2016 Elsevier B.V. All rights reserved.

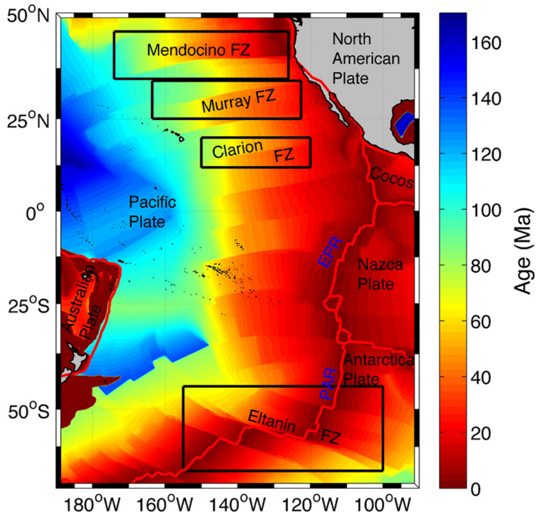

Fig. 1. Age map of the Pacific ocean floor (Müller et al., 2008). Black boxes represent the study areas and red lines denote plate boundaries. EPR: East Pacific Rise, PAR: Pacific-Antarctic Rise and FZ: Fracture Zone. (For interpretation of the references to color in this figure, the reader is referred to the web version of this article.)

the initiation of subduction (Solomatov, 2004). The seismically derived thermal structure of the Pacific lithosphere, which deviates from the standard cooling model, may also constrain the activation energy (Ritzwoller et al., 2004). The lithospheric seismic structure can be explained with thermo-mechanical erosion by convective instabilities with either diffusion creep with the activation energy of $\sim$120 kJ mol^{-1} or dislocation creep with the activation energy of 360–540 kJ mol^{-1} (van Hunen et al., 2005). As pointed out by Korenaga and Korenaga (2008), however, the old Pacific seafloor under which lithospheric thinning is inferred, is heavily populated with hotspot islands and oceanic plateaus, and it is not clear whether the thinning is due to intrinsic convective instabilities. Here we show that a new kind of observational constraint on the activation energy of high-temperature creep can be extracted from the subtle signatures of the geoid along oceanic fracture zones. A recent study of regional geoid anomalies along the Mendocino fracture zone indicates the occurrence of small-scale convective instabilities (Cadio and Korenaga, 2014). Because the amplitude of involved temperature variations can be related to the activation energy, we analyze four major fracture zones in the Pacific (Fig. 1) and provide a new observational constraint on activation energy, by establishing the characteristic amplitude of temperature variations associated with small-scale convection.

2. Data analysis and inversion

Oceanic lithosphere gradually cools and thickens as seafloor ages (Turcotte and Schubert, 2002). Consequently, a fracture zone, which juxtaposes two lithospheric segments of different ages (and thus of different thicknesses), produces lateral density variations detectable in geoid signal (Crough, 1979). Such variations in the thermal structure of oceanic lithosphere could also give rise to convective instabilities at its base (Huang et al., 2003; Dumoulin et al., 2008). This geodynamic process yields an additional geoid component, based on which we can constrain the nature of instabilities. To isolate this additional convective component, we first estimate the geoid contribution of lithospheric cooling from the half-space cooling model (HSC), which linearly relates the thickness of oceanic lithosphere with the square root of seafloor age (Turcotte and Oxburgh, 1967). To that aim, we use the 3D numerical model of oceanic lithosphere developed by Cadio and Korenaga (2012) in order to take into account both vertical and lateral density variations across the fracture zone. An analytical solution for a theoretical geoid exists for the half-space cooling (HSC) model (Haxby and Turcotte, 1978), but it ignores any lateral density perturbations, which is inappropriate especially when considering geoid signals around a fracture zone. Our model of lithosphere, assumed in local isostatic equilibrium, is composed of an array of constant density prisms, for which the density and location are coupled to temperature variations predicted by the HSC model. The values of thermal parameters used in the theoretical calculation are given by Cadio and Korenaga (2012). A geoid signal in every surface point of the model space is calculated by adding contributions from all individual prisms. Among standard evolution models, the HSC model predicts the greatest geoid contribution for old seafloor (Haxby and Turcotte, 1978) and thus gives us the minimal amplitude of residual signals after correction for cooling. Consequently, density contrasts and thermal variations derived from our study can be seen as lower bounds.

The identification of the cooling component in the total geoid is considerably improved here by using the continuous wavelet transform (Cadio and Korenaga, 2014). Such analysis provides a detailed description of signals both in spatial and spectral domains, and thus highlights the signal components at each scale and position. We use spherical Poisson multipole wavelets that are particularly well suited to analyze potential fields (Holschneider et al., 2003). The simultaneous analysis of the EGM2008 geoid (Pavlis et al., 2008) and theoretical geoid in the wavelet domain, at scales varying from 100 to 500 km, shows that the characteristic scale of cooling process in the vicinity of fracture zones is $\sim$100 km. This estimate is relevant because the expected depths of density sources range from the surface to about 100–150 km, which corresponds to the depth extent of oceanic lithosphere.

We apply this approach to four major fracture zones in the Pacific: Mendocino, Clarion, Murray, and Eltanin (Fig. 1). Because of their large age offsets, they display significant geoid signals and are optimal place to initiate convective instabilities. The location and the geometry of these fracture zones also allow us to identify a large number of residual geoid anomalies, covering seafloor as old as 100 Ma (Figs. 1–2 and Figs. S1–S3). We focus only on anomalies localized at 100 km scale, and those satisfying the following two criteria (Cadio and Korenaga, 2014): (1) they are not correlated with any topographic structure (Figs. 2 and S1–S3) and (2) their spectral content indicates an extremum at 100 km scale, ensuring that this spatial scale is characteristic of a signal under consideration (Fig. S4). With this screening, localized residual geoid anomalies may safely be regarded to originate in perturbations to the density structure of normal oceanic lithosphere, not in dynamic or flexural topography. If the lithosphere is treated as purely elastic and the fracture zone behaves as a locked fault, for example, differential subsidence across the fracture zone could indeed deflect the lithosphere, producing a ridge on the younger side and a trough on the older side (Sandwell and Schubert, 1982; Sandwell, 1984). Flexural deformation could contribute to geoid anomalies, but such anomalies would be correlated with flexural topography. Furthermore, the residual geoid anomalies are corrected for locally compensated residual topography assuming Airy compensation (Haxby and Turcotte, 1978), so the crustal contribution to the residual anomalies is minimized. After subtracting this isostatic geoid, we invert the residual anomalies for the statistical distribution of their source density perturbations.

Our inversion method is based on Bayesian statistics and is implemented by combining forward modeling with Markov chain Monte Carlo sampling (Cadio and Korenaga, 2014). We approximate each density perturbation as a right rectangular prism and calculate its geoid signature in a static Earth's mantle by solving the Poisson's equation (e.g. Nagy et al., 2000). We do not account the geoid contribution of the surface topographic deformation potentially induced by the presence of such density per-

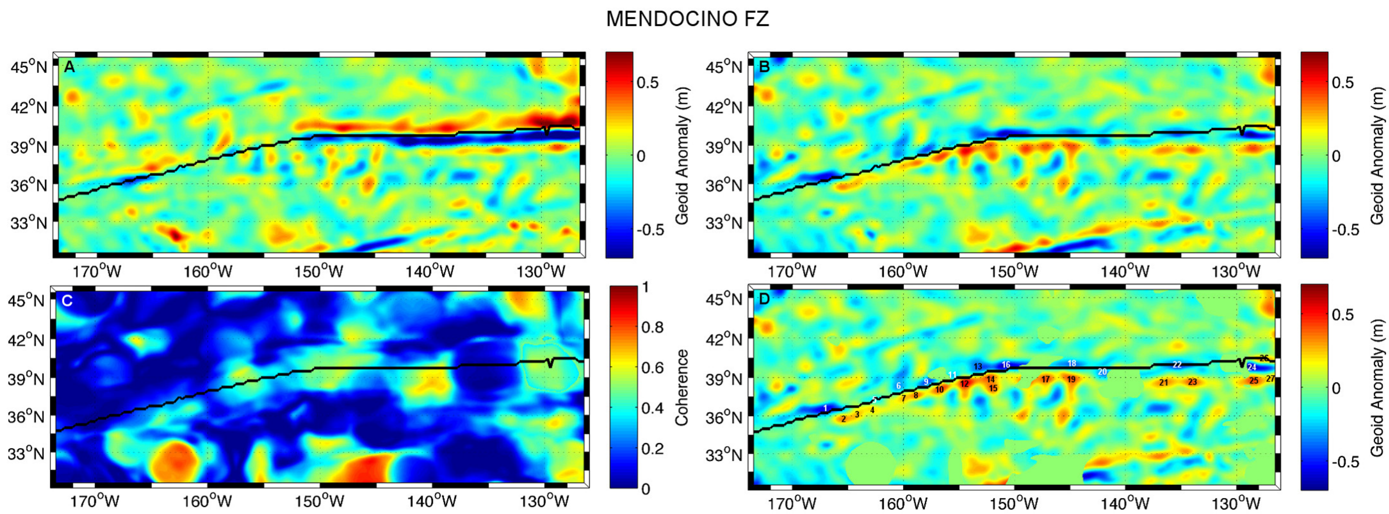

Fig. 2. Selection of geoid anomalies along the Mendocino fracture zone. (A) Localized geoid anomalies at 100 km scale, (B) residual localized geoid anomalies at 100 km scale after correcting for lithospheric cooling and topography, (C) coherence between residual geoid and topography after correcting for lithospheric cooling, and (D) residual geoid anomalies with coherence masking. The location for which the correlation between geoid and topography anomalies is high (>0.5) is masked as 0. The correlation is calculated in each point of the study area following the wavelet method developed in Cadio et al. (2012). Each value of the local coherence is obtained from the geoid and topography wavelet coefficients over a window, the width of which is twice the scale of the wavelet. The significance of the local coherence in the 95% confidence limit is 0.67. By including the effect of the measurement noise on the coherence (Cadio et al., 2012), we thus consider that the geoid and the topography are correlated if the coherence is greater than the lower bound of 0.5. The numbers indicate chosen targets for inversion. Solid lines indicate the locations of the fracture zone.

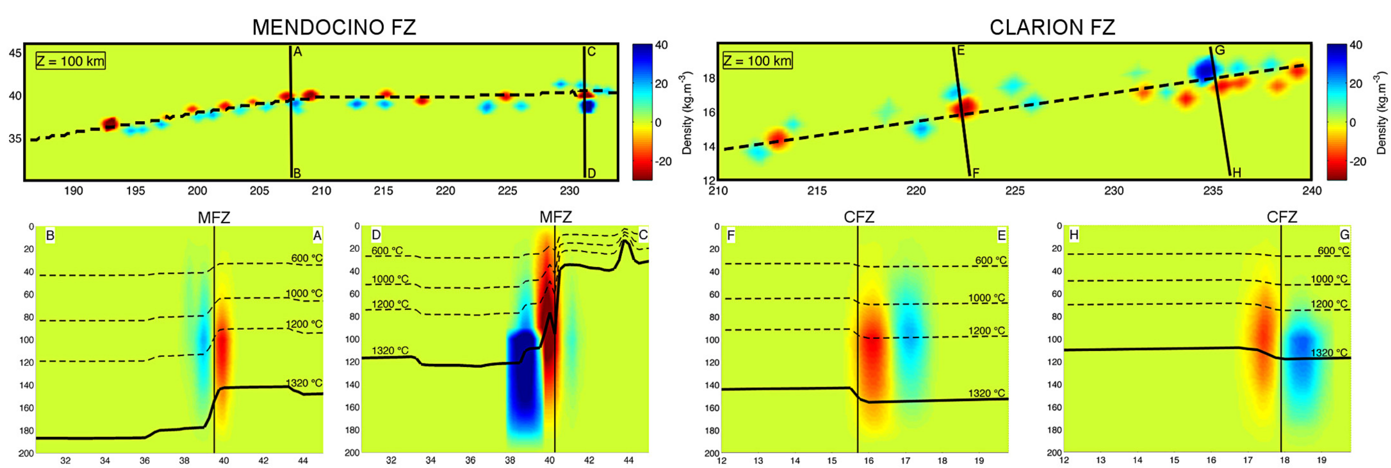

Fig. 3. Distribution of density anomalies along the Mendocino and Clarion fracture zones. (Top) Horizontal cross sections at 100 km depth of the mean density derived from inversions for localized geoid anomalies. (Bottom) Vertical cross sections located along transects shown in the above. Solid lines represent the bottom of thermal lithosphere (as defined by the 1320 °C isotherm) based on the half-space cooling model, and dash lines are other isotherms. The locations of fracture zones (MFZ for Mendocino and CFZ for Clarion) are indicated by vertical lines.

turbation. At 100 km scale, the strength of the lithosphere suppresses a significant amount of dynamic topography signal for a mean elastic thickness greater than 20 km (McKenzie, 2010; Watts et al., 2013). Moreover, we only consider the residual geoid anomalies without correlated topographic signatures. By assuming a simple source body, the number of model parameters is limited to six: the average density of a prism, its lateral and vertical extents, its depth, and its orientation. To be consistent with the residual geoid anomalies to be modeled, theoretical geoid anomalies are also passed through the wavelet transform with the scale of 100 km. The inherent nonuniqueness of such inversion is thus substantially reduced (1) by using spectral localization through the continuous wavelet transform that provides constraints on the depth location and size of sources, and (2) by a priori bounds on the amplitude of density perturbations expected within the convecting mantle (Cadio and Korenaga, 2014). A Markov chain Monte Carlo procedure, with the Metropolis–Hastings algorithm, is then used to efficiently explore the model space and retain the high-probability solutions. The different steps of calculations are detailed in Cadio and Korenaga (2014).

3. Results

Following our criteria, 95 local geoid anomalies are identified along the four fracture zones (Figs. 2 and S1–S3). The solutions of our inversions are distributed over the six-dimensional model space. To better visualize them, we translate the model space into the corresponding three-dimensional physical space and calculate the mean density distribution in each point for all of inverted geoid anomalies. Fig. 3 illustrates the results obtained for the Mendocino and Clarion fracture zones. The results for other fracture zones are given in Fig. S6. The cross-sections at 100 km depth show the distribution of density perturbations along fracture zones, and their vertical extents are closely related to the structure of the lowermost lithosphere. The base of thermal lithosphere (defined at which the temperature reaches the 99% of internal temperature) predicted from the HSC model is also shown as a solid curve

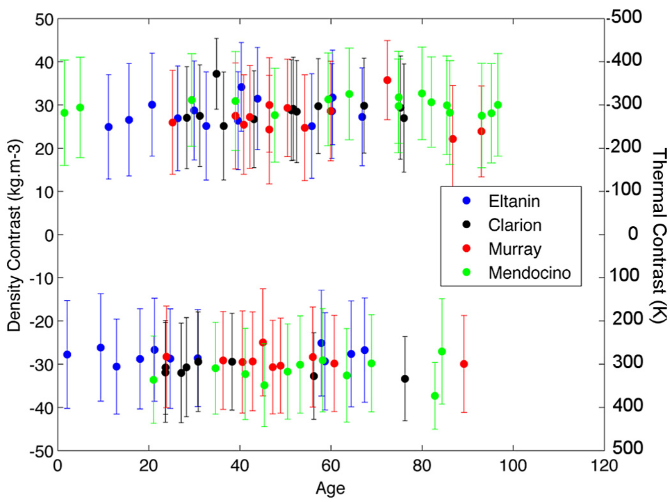

Fig. 4. Mean density contrasts estimated from individual geoid anomalies as a function of seafloor age, for the four fracture zones. The corresponding thermal contrasts are shown on the right. Error bars represent one standard deviation (see Tables S1–S4).

in each panel. Both positive and negative anomalies are located in the vicinity of the base of thermal lithosphere. As a natural result of spectral localization, the horizontal wavelength of inferred density perturbations is also on the order of 100 km, which is still below the resolution of the latest generation of global surface wave tomography (e.g., Schaeffer and Lebedev, 2013). Our approach benefits from the high spatial resolution of the geoid data.

Fig. S5 shows that the lower bound of density perturbations Z_2 is a well-constrained parameter, the solutions of inversions being clustered around a specific value corresponding to the lowermost lithosphere. The upper bound Z_1 is less well defined because of its trade-off with the density contrast (Cadio and Korenaga, 2014). As expected from potential field theory, the amplitude of a geoid anomaly is inversely proportional to the depth of the source density anomaly. In order to counteract such signal attenuation with the source depth, $|\Delta\rho|$ linearly increases with Z_1 in the inversion. However, another high correlation exists between Z_1 and Z_2 so that the most likely solutions for the upper bound are distributed in the lower half of oceanic lithosphere.

The mean density contrast and its uncertainty computed for each geoid anomaly (Tables S1–S4) is shown in Fig. 4 as a function of seafloor age and in Fig. S7 as a function of age offset across fracture zone. The mean amplitude is about 30 ± 10 kg m^{-3} for the positive anomalies and about -30 ± 10 kg m^{-3} for the negative anomalies. These values are remarkably consistent irrespective of seafloor age and age offsets, for all of the four fracture zones analyzed. This magnitude of density perturbation should be regarded as a lower bound, not only because we use the HSC model as a reference, but also because we place a priori bounds of ± 50 kg m^{-3} in our inversion (Cadio and Korenaga, 2014). We also note that it is more difficult to find solutions with density perturbations smaller than ± 20 kg m^{-3} (Fig. S5) and thus with Z_1 in the uppermost lithosphere.

4. Discussion

Density perturbations in oceanic lithosphere can be related to (1) lateral compositional differences triggered by alteration reactions/dehydration or (2) temperature variations. Alteration effects such as serpentinization are prominent only above the 600 °C isotherm (Ulmer and Trommsdorff, 1995) and would thus be confined to the upper part of the lithosphere. The location and geometry of these density anomalies thus seem to be most consistent with the occurrence of thermal convective instabilities at the base of oceanic lithosphere. Small-scale convection (SSC) could develop beneath old seafloor by gravitational instabilities of the thickened cold lithosphere but also under young seafloor if mantle viscosity is low enough (Buck and Parmentier, 1986; Korenaga and Jordan, 2003) or there exists lateral thermal variation due to a fracture zone (Huang et al., 2003; Dumoulin et al., 2008). At the onset, the typical wavelength of SSC in numerical simulations (Huang et al., 2003; van Hunen et al., 2005; Dumoulin et al., 2008) is around 200 km, which is in agreement with the spatial organization of density anomalies derived from our inversion.

When convective instabilities take place, cold downwellings lead to the local thickening of lithosphere, resulting in positive density perturbations. Conversely, hot upwellings induce the thinning of lithosphere by delamination, resulting in the partial replacement of lithosphere with hot asthenospheric material, which leads to negative density perturbations. According to numerical predictions (Huang et al., 2003; Dumoulin et al., 2008), the cold downwellings are located near the fracture zone but are slightly shifted to its older side. Such positive density perturbations can be seen on the older side along the four fracture zones investigated here (Figs. 3 and S6). The upwellings tend to develop below the younger lithosphere and this prediction is also generally compatible with the locations of the observed negative density anomalies. Also, edge-driven flow across a fracture zone can thermally erode the basal relief of the lithosphere (Dumoulin et al., 2008) and deviate the lithospheric thickness step toward the older side of the fracture zone. Consequently, low-density perturbations can be also observed below the fracture zone on the older side. The discontinuous pattern of density perturbations is also in agreement with the time-dependent nature of convective instabilities.

Assuming such a purely thermal origin, a density anomaly can be converted to a temperature anomaly through the thermal expansion coefficient, for which 3×10^{-5} K is assumed in this study. The corresponding thermal contrasts are indicated in Fig. 4. The amplitude of density anomalies derived from our inversion requires mean temperature variations of as large as 300 ± 100 K. This temperature contrast is also consistent with the vertical extent of density perturbations, which indicates the erosion of lithosphere up to the isotherm of ∼1000 °C (Fig. 3 and Fig. S6); the delamination of lithospheric mantle with temperatures from 1300 °C to 1000 °C can explain both the amplitude of density anomalies and their depth extents. SSC disrupts the thermal and compositional stratification of the uppermost mantle and can thus induce melting. The positive thermal anomalies in SSC upwellings are usually insufficient to trigger melting in a depleted harzburgite layer, which already experienced mid-ocean ridges melting. However, immediately after its onset, SSC removes this depleted layer in downgoing sheets and replaces it with a fresh mantle from below, allowing subsequent melting. With normal potential temperature (i.e., ∼1350 °C), upwelling mantle exceeds its dry solidus at the depth of 70 km and starts to melt (e.g., Langmuir et al., 1992). Our inversion results suggest (Fig. 3 and Fig. S6) that lithosphere may be thinned down to ∼50 km at some places. The vertical extent for partial melting is thus only 20 km, for which the average degree of partial melting would be 2–3%. The total amount of melt that could be produced depends on the pattern of mantle flow associated with lithospheric thinning. Melt migration through the rest of lithosphere may not be very efficient because, unlike a mantle plume, upwelling due to lithospheric thinning is a one-time event. Consequently, melt generated by thinning could largely fail to reach the surface owing to its thermal interaction with cold lithosphere (Yamamoto et al., 2014).

The amplitude of temperature perturbation caused by SSC can be directly related to the rheology of oceanic lithosphere.

With the assumption of Newtonian rheology (diffusion creep), when the activation energy is ∼375 kJ mol^{-1} as determined from laboratory studies on dry olivine (Mei and Kohlstedt, 2000a; Hirth and Kohlstedt, 2003), only the very bottom of lithosphere can delaminate, and the expected amplitude of temperature variations in SSC is only ∼100 K (Korenaga and Jordan, 2002; 2004). To explain the amplitude of as high as 300 ± 100 K, the activation energy must be lowered to ∼100 ± 50 kJ mol^{-1}. Although diffusion creep should dominate for the onset of SSC (e.g., Korenaga and Jordan, 2002), the steep lateral thermal gradient across the fracture zone could trigger dislocation creep from the beginning. For some geodynamical problems, non-Newtonian rheology (dislocation creep) may be approximated with Newtonian rheology (Christensen, 1984; Solomatov and Moresi, 2000). Using the scaling of Solomatov and Moresi, an activation energy of 100 ± 50 kJ mol^{-1} for diffusion creep is equivalent to an activation energy of 225 ± 112 kJ mol^{-1} for dislocation creep (with the stress exponent of 3.5).

Such activation energy is too low to be consistent with the rheology of olivine aggregates (Karato and Wu, 1993; Hirth and Kohlstedt, 2003; Korenaga and Karato, 2008). Our new estimate of the activation energy thus implies that the rheology of oceanic lithosphere is not well represented by that of pure olivine aggregates. In fact, a recent laboratory experiment suggests that the presence of a secondary phase such as orthopyroxene is important for rheological weakening (Farla et al., 2013), and our estimate of ∼100 ± 50 kJ mol^{-1} (or 225 ± 112 kJ mol^{-1} for dislocation creep) may represent the 'effective' activation energy for such polymineralic aggregates. Whereas the results of our geoid inversion themselves do not distinguish between diffusion and dislocation creep, we suspect that dislocation creep would be more appropriate to explain the inferred occurrence of SSC around the fracture zones. If the activation energy of diffusion creep were indeed as low as 100 kJ mol^{-1}, the growth of oceanic lithosphere would be severely limited because SSC could take place from infinitesimal perturbations. The onset of SSC with dislocation creep, however, requires finite initial amplitude (e.g., Solomatov and Barr, 2007) and thus special conditions, such as fracture zone heterogeneities and plume impingements. This can also be understood from Fig. 5; effective viscosity for dislocation creep would be too high to initiate SSC when the stress level is low. This selective occurrence of SSC by dislocation creep has also been suggested by the analysis of the depth-age relation of seafloor (Korenaga, 2015). In other words, the activation energy for diffusion creep is probably still around 300 kJ mol^{-1}, but that for dislocation creep may be as low as ∼200 kJ mol^{-1}. The evolution of normal oceanic lithosphere would be governed by the former, but when the lithosphere is subject to high stresses, the latter becomes relevant. Though the low activation energy alone is insufficient to prevent stagnant-lid convection (Solomatov, 1995), the thickness of the stiffest core of the lithosphere, represented by the region with high yield stress (> a few hundred MPa), would be considerably reduced (Fig. 5). It is thus worth exploring the impact of this low activation energy on the initiation of plate tectonics, in combination with other weakening mechanisms. The stiffest core seen in Fig. 5, for example, is restricted to the low-temperature domain (<500 °C), where thermal cracking is most effective (Korenaga, 2007). Composite rheology, i.e., the combination of diffusion and dislocation creep, has often been considered in geodynamical modeling (e.g., van Hunen et al., 2005), but given that even the rheology of olivine, which is undoubtedly best understood among mantle minerals, suffers from considerable uncertainty (Korenaga and Karato, 2008; Mullet et al., 2015), existing numerical studies have explored only a very small fraction of the model parameter space. Our study provides a new kind of observational constraint on the macroscopic strength of oceanic lithosphere, which should prove important for future modeling studies with composite rheology.

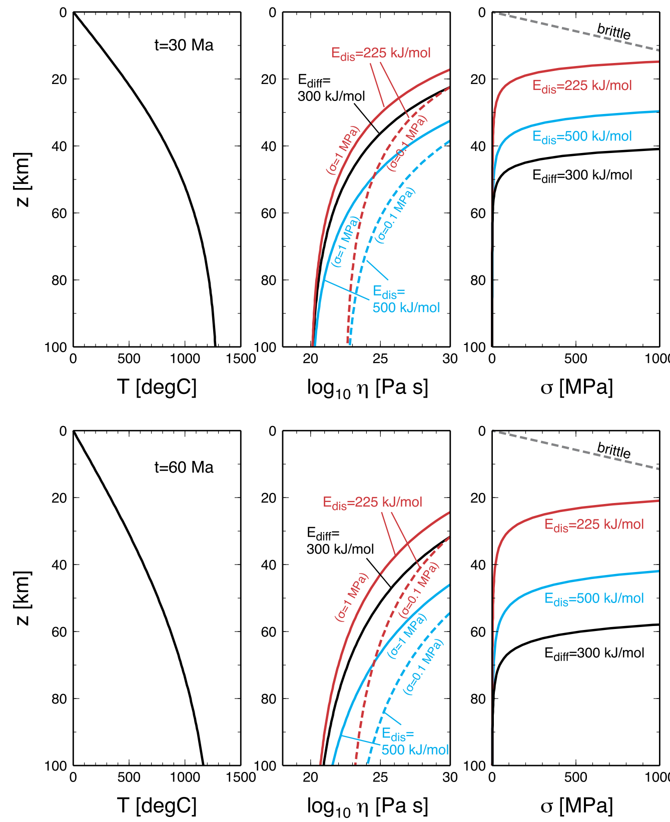

Fig. 5. Strength of oceanic lithosphere. (Left) temperature profile, (middle) effective viscosity, and (right) yield stress with the strain rate of 10^{-15} s^{-1}. The temperature profile is calculated using the standard half-space cooling solution (Turcotte and Schubert, 2002) with the temperature difference of 1350 K and the thermal diffusivity of 10^{-6} m^2 s^{-1}. Here mantle viscosity is assumed to be in the form of $\eta(T) \propto \sigma^{1-n} \exp(E/RT)$, where σ is stress, n is stress exponent, E is activation energy, and R is the universal gas constant. Viscosity is scaled so that it takes the reference viscosity of 10^{20} Pa s at $T = 1573$ K; taking the reference at this temperature is appropriate given that the deformation experiments of olivine aggregates are conducted at 1450–1600 K (Fig. 3 of Korenaga and Karato, 2008). The cases of diffusion creep ($n = 1$) and dislocation creep ($n = 3.5$) are shown. Effective viscosity for dislocation creep depends on stress, and the stress of 1 MPa is used as the reference stress here. The upper panels are for 30-Ma-old lithosphere, and the lower panels for 60-Ma-old lithosphere. In the middle and right panels, the case of diffusion creep with E of 300 kJ mol^{-1} is shown in black, and the cases of dislocation creep with E of 500 kJ mol^{-1} and 225 kJ mol^{-1} are shown in blue and red, respectively. Shown in dashed lines in the middle panel are the cases of dislocation creep with the stress of 0.1 MPa. In the right panel, the yield stress corresponding to brittle deformation is shown in dashed gray line. (For interpretation of the references to color in this figure, the reader is referred to the web version of this article.)

Our inference on mantle rheology may also be extended to the dynamics of continental lithosphere. The subcontinental lithospheric mantle has more complex histories than the oceanic counterpart, exhibiting a greater range of depletion (e.g., Boyd, 1989) and a variety of metasomatic processes (e.g., Kelemen et al., 1998), so the direct application of our finding would be limited. Nonetheless, the possibility of substantial lithospheric delamination by low activation energy would still be important when considering the long-term stability of continental lithosphere (e.g., O'Reilly et al., 2001; West et al., 2009). Future studies on the role of composite rheology in the dynamics of continental lithosphere are warranted, especially with consideration of the uncertainty of rheological parameters (e.g., Chu and Korenaga, 2012).

Acknowledgements

We are grateful to two anonymous reviewers for critical and constructive comments on the manuscript. This work was supported in part by the facilities and staff of the Yale University Faculty of Arts and Sciences High Performance Computing Center.

Appendix A. Supplementary material

Supplementary material related to this article can be found online at http://dx.doi.org/10.1016/j.epsl.2016.05.027.

References

Bercovici, D., Ricard, Y., Richards, M.A., 2000. The relation between mantle dynamics and plate tectonics: a primer. In: Richards, M.A., Gordon, R., van der Hilst, R. (Eds.), The History and Dynamics of Global Plate Motions. In: Geophys. Monogr. Ser. Am. Geophys. Union, vol. 121, pp. 5–46.
Bercovici, D., 2003. The generation of plate tectonics from mantle convection. Earth Planet. Sci. Lett. 205, 107–121.
Boyd, F.R., 1989. Compositional distinction between oceanic and cratonic lithosphere. Earth Planet. Sci. Lett. 96, 15–26.
Braun, J., Chery, J., Poliakov, A., Mainprice, D., Vauchez, A., Tomassi, A., Daignieres, M., 1999. A simple parameterization of strain localization in the ductile regime due to grain size reduction: a case study for olivine. J. Geophys. Res. 104, 25167–25181.
Buck, W.R., Parmentier, E.M., 1986. Convection beneath young oceanic lithosphere: implications for thermal structure and gravity. J. Geophys. Res. 91, 1961–1974.
Cadio, C., Ballmer, M., Panet, I., Diament, M., Ribe, N., 2012. New constraints on the origin of the Hawaiian swell from wavelet analysis of the geoid to topography ratio. Earth Planet. Sci. Lett. 359–360, 40–54.
Cadio, C., Korenaga, J., 2012. Localization of geoid anomalies and the evolution of oceanic lithosphere: a case study from the Mendocino Fracture Zone. J. Geophys. Res. 117, B10404. http://dx.doi.org/10.1029/2012JB009524.
Cadio, C., Korenaga, J., 2014. Resolving the fine-scale density structure of shallow oceanic mantle by Bayesian inversion of localized geoid anomalies. J. Geophys. Res. 119, 3627–3645. http://dx.doi.org/10.1002/2013JB010840.
Christensen, U.R., 1984. Convection with pressure and temperature dependent non-Newtonian rheology. Geophys. J. R. Astron. Soc. 77, 242–284.
Chu, X., Korenaga, J., 2012. Olivine rheology, shear stress, and grain growth in the lithospheric mantle: geological constraints from the Kaapvaal craton. Earth Planet. Sci. Lett. 333–334, 52–62.
Crough, S.T., 1979. Geoid anomalies across fracture zones and the thickness of the lithosphere. Earth Planet. Sci. Lett. 44, 224–230.
Dumoulin, C., Choblet, G., Doin, M.P., 2008. Convective interactions between oceanic lithosphere and asthenosphere: influence of a transform fault. Earth Planet. Sci. Lett. 274, 301–309.
Farla, R.J.M., Karato, S., Cai, Z., 2013. Role of orthopyroxene in rheological weakening of the lithosphere via dynamic recrystallization. Proc. Natl. Acad. Sci. USA 110, 16355–16360.
Goetze, C., Evans, B., 1979. Stress and temperature in the bending lithosphere as constrained by experimental rock mechanics. Geophys. J. R. Astron. Soc. 59, 463–478.
Gurnis, M., Hall, C.E., Lavier, L., 2004. Evolving force balance during incipient subduction. Geochem. Geophys. Geosyst. 5, Q07001. http://dx.doi.org/10.1029/2003GC000681.
Hall, C.E., Gurnis, M., Sdrolias, M., Lavier, L.L., Muller, R.D., 2003. Catastrophic initiation of subduction following forced convergence across fracture zones. Earth Planet. Sci. Lett. 212, 15–30. http://dx.doi.org/10.1016/S0012-821X(03)00242-5.
Haxby, W.F., Turcotte, D.L., 1978. On isostatic geoid anomalies. J. Geophys. Res. 83, 5473–5478.
Hirth, G., Kohlstedt, D., 2003. Rheology of the upper mantle and the mantle wedge: a view from the experimentalists. In: Eiler, J. (Ed.), Inside the Subduction Factory. In: Geophys. Monogr. Ser., vol. 138. Am. Geophys. Union, pp. 83–105.
Holschneider, M., Chambodut, A., Mandea, M., 2003. From global to regional analysis of the magnetic field on the sphere using wavelet frames. Phys. Earth Planet. Inter. 135, 107–124.
Huang, J., Zhong, S., van Hunen, J., 2003. Controls on sublithospheric small-scale convection. J. Geophys. Res. 108 (B8), 2405. http://dx.doi.org/10.1029/2003JB002456.
Kameyama, M., Yuen, D., Fujimoto, H., 1997. The interaction of viscous heating with grain-size dependent rheology in the formation of localized slip zones. Geophys. Res. Lett. 24, 2523–2526.
Karato, S., Wu, P., 1993. Rheology of the upper mantle: a synthesis. Science 260, 771–778.
Karato, S.I., Jung, H., 2003. Effects of pressure on high-temperature dislocation creep in olivine. Philos. Mag. 83 (3), 401–414.
Kelemen, P.B., Hart, S.R., Bernstein, S., 1998. Silica enrichment in the continental upper mantle via melt/rock reaction. Earth Planet. Sci. Lett. 164, 387–406.
Korenaga, J., Jordan, T.H., 2002. On 'steady-state' heat flow and the rheology of oceanic mantle. Geophys. Res. Lett. 29 (22), 2056. http://dx.doi.org/10.1029/2002GL016085.
Korenaga, J., Jordan, T.H., 2003. Physics of multiscale convection in Earth's mantle: onset of sublithospheric convection. J. Geophys. Res. 108 (B7), 2333. http://dx.doi.org/10.1029/2002JB001760.
Korenaga, J., Jordan, T.H., 2004. Physics of multiscale convection in Earth's mantle: evolution of sublithospheric convection. J. Geophys. Res. 109, B01405. http://dx.doi.org/10.1029/2003JB002464.
Korenaga, J., 2007. Thermal cracking and the deep hydration of oceanic lithosphere: a key to the generation of plate tectonics? J. Geophys. Res. 112, B05408. http://dx.doi.org/10.1029/2006JB004502.
Korenaga, J., Karato, S., 2008. A new analysis of experimental data on olivine rheology. J. Geophys. Res. 113, B02403. http://dx.doi.org/10.1029/2007JB005100.
Korenaga, T., Korenaga, J., 2008. Subsidence of normal oceanic lithosphere, apparent thermal expansivity, and seafloor flattening. Earth Planet. Sci. Lett. 268, 41–51.
Korenaga, J., 2013. Initiation and evolution of plate tectonics on Earth: theories and observations. Annu. Rev. Earth Planet. Sci. 41, 117–151.
Korenaga, J., 2015. Seafloor topography and the thermal budget of Earth. In: Fouger, G.R., Lustrino, M., King, S.D. (Eds.), The Interdisciplinary Earth: A Volume in Honor of Don L. Anderson. In: GSA special paper 514 and AGU Special Publication, vol. 71, pp. 167–185.
Landuyt, W., Bercovici, D., Ricard, Y., 2008. Plate generation and two-phase damage theory in a model of mantle convection. Geophys. J. Int. 174, 1065–1080.
Langmuir, C.H., Klein, E.M., Plank, T., 1992. Petrological systematics of mid-ocean ridge basalts: constraints on melt génération beneath ocean ridges. In: Phipps Morgan, J., Blackman, D.K., Sinton, J.M. (Eds.), Mantle Flow and Melt Generation at Mid-Ocean Ridges. In: Geophys. Monogr. Ser. Am. Geophys. Union, pp. 183–280.
McKenzie, D., 2010. The influence of dynamically supported topography on estimates of Te. Earth Planet. Sci. Lett. 295 (1–2), 127–138. http://dx.doi.org/10.1016/j.epsl.2010.03.033.
Mei, S., Kohlstedt, D.L., 2000a. Influence of water on plastic deformation of olivine aggregates: 1. Diffusion creep regime. J. Geophys. Res. 105, 21,457–21,469.
Mei, S., Kohlstedt, D.L., 2000b. Influence of water on plastic deformation of olivine aggregates: 2. Dislocation creep regime. J. Geophys. Res. 105, 21,471–21,481.
Müller, R.D., Sdrolia, M., Gaina, C., Roest, W.R., 2008. Age, spreading rates, and spreading asymmetry of the world's ocean crust. Geochem. Geophys. Geosyst. 9, Q04006. http://dx.doi.org/10.1029/2007GC001743.
Mullet, B.G., Korenaga, J., Karato, S.-I., 2015. Markov chain Monte Carlo inversion for the rheology of olivine single crystals. J. Geophys. Res., Solid Earth 120, 3142–3172. http://dx.doi.org/10.1002/2014JB011845.
Nagy, D., Papp, G., Benedek, J., 2000. The gravitational potential and its derivatives for the prism. J. Geod. 74, 552–560.
O'Reilly, S.Y., Griffin, W.L., Djomani, Y.H., Morgan, P., 2001. Are lithospheres forever? Tracking changes in subcontinental lithospheric mantle through time. GSA Today 11, 4–10.
Pavlis, N., Holmes, S.A., Kenyon, S.C., Factor, J.K., 2008. An Earth gravitational model to degree 2160: EGM2008, presented at the 2008 General Assembly of the European Geosciences Union, Vienna, April 13–18.
Regenauer-Lieb, K., Yuen, D.A., Branlund, J., 2001. The initiation of subduction: criticality by addition of water. Science 294, 578–580. http://dx.doi.org/10.1126/science.1063891.
Ritzwoller, M.H., Shapiro, N.M., Zhong, S., 2004. Cooling history of the Pacific lithosphere. Earth Planet. Sci. Lett. 226, 69–84.
Sandwell, D.T., Schubert, G., 1982. Lithospheric flexure at fracture zones. J. Geophys. Res. 87, 4657–4667.
Sandwell, D.T., 1984. Thermomechanical evolution of oceanic fracture zones. J. Geophys. Res. 89, 11,401–11,413.
Schaeffer, A.J., Lebedev, S., 2013. Global shear speed structure of the upper mantle and transition zone. Geophys. J. Int. 194, 417–449.
Schubert, G., Turcotte, D.L., Olson, P., 2001. Mantle Convection in the Earth and Planets. Cambridge University Press, New York.
Solomatov, V.S., 1995. Scaling of temperature- and stress-dependent viscosity convection. Phys. Fluids 7, 266–274.
Solomatov, V.S., Moresi, L.-N., 2000. Scaling of time-dependent stagnant lid convection: application to small-scale convection on the Earth and other terrestrial planets. J. Geophys. Res. 105, 21,795–21,818.
Solomatov, V.S., 2004. Initiation of subduction by small-scale convection. J. Geophys. Res. 109, B01412. http://dx.doi.org/10.1029/2003JB002628.
Solomatov, V.S., Barr, A.C., 2007. Onset of convection in fluids with strongly temperature-dependent, power-law viscosity, 2, dependence on the initial perturbation. Phys. Earth Planet. Inter. 165, 1–13.
Tackley, P.J., 2000. Mantle convection and plate tectonics: toward an integrated physical and chemical theory. Science 288, 2002–2007.
Toth, J., Gurnis, M., 1998. Dynamics of subduction initiation at pre-existing fault zones. J. Geophys. Res. 103, 18,053–18,067. http://dx.doi.org/10.1029/98JB01076.
Turcotte, D.L., Oxburgh, E.R., 1967. Finite amplitude convective cells and continental drift. J. Fluid Mech. 28, 29–42. http://dx.doi.org/10.1017/S0022112067001880.

Turcotte, D., Schubert, G., 2002. Geodynamics, second ed. Cambridge Univ. Press, Cambridge, U.K.
Ulmer, P., Trommsdorff, V., 1995. Serpentine stability to mantle depths and subduction-related magmatism. Science 268, 858–861.
van Hunen, J., Zhong, S., Shapiro, N.M., Ritzwoller, M.H., 2005. New evidence for dislocation creep from 3-D geodynamic modelling of the Pacific upper mantle structure. Earth Planet. Sci. Lett. 238 (1–2), 146–155.
Watts, A.B., Zhong, S., 2000. Observations of flexture and the rheology of oceanic lithosphere. Geophys. J. Int. 142, 855–875.
Watts, A.B., Zhong, S.J., Hunter, J., 2013. The behavior of the lithosphere on seismic to geologic timescales. Annu. Rev. Earth Planet. Sci. 41, 443–468. http://dx.doi.org/10.1146/annurev-earth-042711-105457.
West, J.D., Fouch, M.J., Roth, J.B., Elkins-Tanton, L.T., 2009. Vertical mantle flow associated with a lithospheric drip beneath the Great Basin. Nat. Geosci. 2, 439–444.
Yamamoto, J., Korenaga, J., Hirano, N., Kagi, H., 2014. Melt-rich lithosphere–asthenosphere boundary inferred from petit-spot volcanoes. Geology 42, 967–970.